Following Structural Changes by Thermal Denaturation using Trapped Ion Mobility Spectrometry – Mass Spectrometry

Kevin Jeanne Dit Fouque[†] and Francisco Fernandez-Lima*,^{†,‡}

ABSTRACT: The behavior of biomolecules as a function of the solution temperature is often crucial to assess their biological activity and function. While heat-induced changes of biomolecules are traditionally monitored using optical spectroscopy methods, their conformational changes and unfolding transitions remain challenging to interpret. In the present work, the structural transitions of bovine serum albumin (BSA) in native conditions (100 mM aqueous ammonium acetate) were investigated as a function of the starting solution temperature (T = -23-70 °C) using a temperature-controlled nanoelectrospray ionization source (nESI) coupled to a trapped ion mobility spectrometry – mass spectrometry (TIMS-MS) instrument. The charge state distribution of the monomeric BSA changed from a native-like, narrow charge state ($[M + 12H]^{12+} - [M + 16H]^{16+}$ at -23 °C) and narrow mobility distribution towards an unfolded-like, broad charge state (up to $[M + 46H]^{46+}$ at -70 °C) and broad mobility distribution. Inspection of the average charge state and CCS distribution suggested a two-state unfolding transition with a melting temperature $T_m - 56 \pm 1$ °C; however, the inspection of the CCS profiles at the charge state level as a function of the solution temperature showcase at least six structural transitions (T1-T7). If the starting solution concentration is slightly increased (from 2 to 25 μ M), this method can detect non-specific BSA dimers and trimers who dissociate early ($T_d - 34 \pm 1$ °C) and may disturb the melting curve of the BSA monomer. In a single experiment, this technology provides a detailed view of the solution, protein structural landscape (mobility vs solution temperature vs relative intensity for each charge state).

Globular proteins are known to adopt folded, compact structures in their native states. The native state(s) can be altered by chaotropic agents¹⁻³ (e.g. guanidinium chloride) as well as changes in pH,^{1, 4, 5} organic solvent^{1, 6} and temperature.^{1, 7, 8} These conformational changes are traditionally monitored in solution using a variety of technique such as, calorimetry,^{9, 10} fluorescence,^{11, 12} circular dichroism^{13, 14} and nuclear magnetic resonance.^{15, 16}

Mass spectrometry has demonstrated the ability to follow protein solution structural changes based on the changes in the charge state distributions (e.g., induced by changes in pH and/or organic solvent conditions).¹⁷⁻¹⁹ In addition, the capability to control the solution temperature prior to ESI-MS has allowed to investigate thermally induced protein structural changes.20-25 ESI-MS has provided a description of the ensemble average structure; while a protein thermal denaturation typically involves several intermediate structures. Moreover, ESI-MS when complemented with ion mobility spectrometry (ESI-IMS-MS), provides a more detail description of the protein conformational changes as a function of the starting molecular environment.26-35 Recent IMS-MS reports have shown the advantages of changing the molecular environment in solution (e.g., pH26-29 and organic content³⁰⁻³⁴) and in the gas phase (e.g., introducing bath gas modifiers³³⁻³⁵) as a way to sample the conformational landscape. Thermal sampling of the protein starting solutions has demonstrated to be powerful in understanding structural transitions and stability of biomolecules.³⁶⁻⁴³ The advantage of the evaporative cooling of the solvent during the ESI process results in the freezing of intermediate states accessible at different solution temperatures. Thermal sampling followed by ESI-IMS-MS provides crucial insights on the protein structural landscape.

In the present work, for the first time, a temperature-controlled nano-ESI source was coupled to second generation trapped ion mobility spectrometry – mass spectrometry (TIMS-TOF MS) instrument for the study of bovine serum albumin (BSA, 66 kDa) solution structural landscape. The high trapping efficiency and extended mass range of the convex electrode TIMS geometry⁴⁴⁻⁴⁶ enabled the inspections of native BSA at low charge states (+12 to +16) as well as non-specific BSA dimers and trimers from relatively low solution concentrations. In the following discussion, a special emphasis is placed on the TIMS-MS capability to follow structural changes of BSA as a function of the starting solution temperature (~23-70 °C) based on the mobility

[†] Department of Chemistry and Biochemistry, Florida International University, Miami, FL 33199, United States.

[‡] Biomolecular Sciences Institute, Florida International University, Miami, FL 33199, United States.

profiles at the charge state level. The observation of several solution intermediate structures before reaching the unfolded state is described.

EXPERIMENTAL SECTION

Materials and Reagents. Bovine serum albumin (BSA, 66 kDa) was obtained from Sigma-Aldrich (Saint-Louis, MO). Ammonium acetate (NH $_4$ Ac) was purchased from Fisher Scientific (Pittsburgh, PA). BSA solutions were analyzed at two concentrations (i.e., 2 μ M and 25 μ M in 100 mM aqueous NH $_4$ Ac). Low concentration Tuning Mix standard (G1969-85000) was used for mobility and mass calibration purposes and obtained from Agilent Technologies (Santa Clara, CA).

Temperature Dependent Electrospray Ionization. Nano-ESI (nESI) emitters were pulled from quartz capillaries (O.D. = 1.0 mm and I.D. = 0.70 mm) using Sutter Instruments Co. P2000 laser puller (Sutter Instruments, Novato, CA). The starting solution temperatures of the nESI emitters were controlled using a custom-made variable temperature emitter holder (Figure S1). The pulled glass capillaries were housed in a thermally conductive aluminum holder equipped with a resistive heater and a K-type thermocouple (± 1 °C). The entire apparatus was brought to temperature by increasing the heater temperature (~23-70 °C) under a constant flow of nitrogen. A voltage of 700- 1200 V relative to the instrument inlet was applied via a tungsten wire inserted into the nESI emitters. Data were obtained using a short temperature gradient (0.13-0.22 °C/s, Figure S2) and the resulted temperatures represent an average every 2-3 °C. The IMS-MS signal was summed at a rate of measurements/second depending 7-15 temperature gradient, such that 100 IMS-MS acquisitions per temperature point were recorded.

TIMS-MS Instrumentation. Ion mobility experiments were performed on a custom built nanoESI-TIMS coupled to an Bruker Impact Q-ToF mass spectrometer (Bruker Daltonics Inc., Billerica, MA, Figure S₁).⁴⁷ Briefly, the ion mobility separation in a TIMS device is based on holding the ions stationary using an electric field (E) against a moving buffer gas (Figure S1).48 In the present design, the TIMS analyzer section is composed of a convex, quadrupolar electrode geometry, as described elsewhere.44 The TIMS unit is controlled by an in-house LabView software (National Instruments) synchronized with the TOF MS platform controls.⁴⁷ TIMS-MS experiments were carried out using nitrogen (N_2) as buffer gas, at ambient temperature (T). The gas velocity was kept constant between the funnel entrance $(P_1 = 2.6 \text{ mbar})$ and exit $(P_2 = 1.1 \text{ mbar})$, Figure S₁) regardless of the starting solution temperatures. An rf voltage of 250 Vpp at 450 kHz was applied to all electrodes. Ions were "softly transferred" from the nESI

source and injected into the TIMS analyzer to avoid potential activation. A low ΔV ($\Delta V = 20$ V) between the deflector (V_{def}) and the funnel entrance (V_{fun}) as well as between the funnel entrance and the TIMS analyzer (V_{ramp}) was used to generate native-like mobility distributions (Figure S1). A V_{def} of -100 V, a V_{fun} of -120 V, base voltage (V_{out}) of 60 V for a V_{ramp} at -140 to -40 V were used for all experiments. The scan rate was 0.95 V/ms. These "soft" ion transmission and trapping conditions guarantee native TIMS measurements.⁴⁹

CCS determination from TIMS-MS experiments. The general fundamentals of TIMS as well as the calibration procedure have been described in the literature. 50-53 Briefly, TIMS separation depends on the gas flow velocity (v_g) , elution voltage (V_e) , ramp time (t_{ramp}) and base voltage (V_{out}) . The reduced mobility, K_o , is defined by:

$$K_0 = \frac{v_g}{E} \cong \frac{A}{(V_e - V_{out})} \qquad \textbf{(1)}$$

where, A is a constant related to the velocity of the bath gas (v_g) define by P_1 and P_2 and the TIMS geometry. The total analysis time (t_{Total}) is given by:

$$t_{Total} = t_{trap} + \left(\frac{v_e}{v_{ramp}}\right) t_{ramp} + tof = t_0 + \left(\frac{v_e}{v_{ramp}}\right) t_{ramp}$$
 (2), where, t_{trap} is the thermalization/trapping time, tof is

(2), where, t_{trap} is the thermalization/trapping time, tof is the time after the ion mobility separation, and V_{ramp} and t_{ramp} are the voltage range and time required to vary the electric field, respectively. The elution voltage (V_e) is experimentally determined by varying the ramp time for a constant ramp voltage. A linear dependence of t_{Total} with t_{ramp} for all the investigated m/z was obtained. From the slope and the intercept of this graph, t_o and V_e can be determined for each m/z range of interest. Reduced mobility values (K_o) were correlated with collision cross section (Ω , \mathring{A}^2) using the Mason-Schamp equation:

$$\Omega = \frac{(18\pi)^{1/2}}{16} \frac{z}{(k_B T)^{1/2}} \left[\frac{1}{m_i} + \frac{1}{m_b} \right]^{1/2} \frac{1}{K_0} \frac{1}{N^*}$$
 (3)

where, z is the charge of the ion, k_B is the Boltzmann constant, N^* is the number density of the bath gas and m_i and m_b refer to the masses of the ion and bath gas, respectively.⁵⁴

RESULTS AND DISCUSSION

Charge state distribution dependence on starting solution temperature. The mass spectrometry analysis of BSA at 2 μ M under native starting solution conditions (i.e., 100 mM NH₄Ac at ~23 °C) exhibited a narrow charge state distribution centered at 14+ (Figure 1a), ranging from [M + 12H]¹²⁺ to [M + 16H]¹⁶⁺. A dependence of the charge state distribution with the starting solution temperature was observed (Figures 1a and 1b). As the starting solution temperature increases, the charge state distribution remained unchanged until ~50 °C, from where a shift toward higher charge states was observed

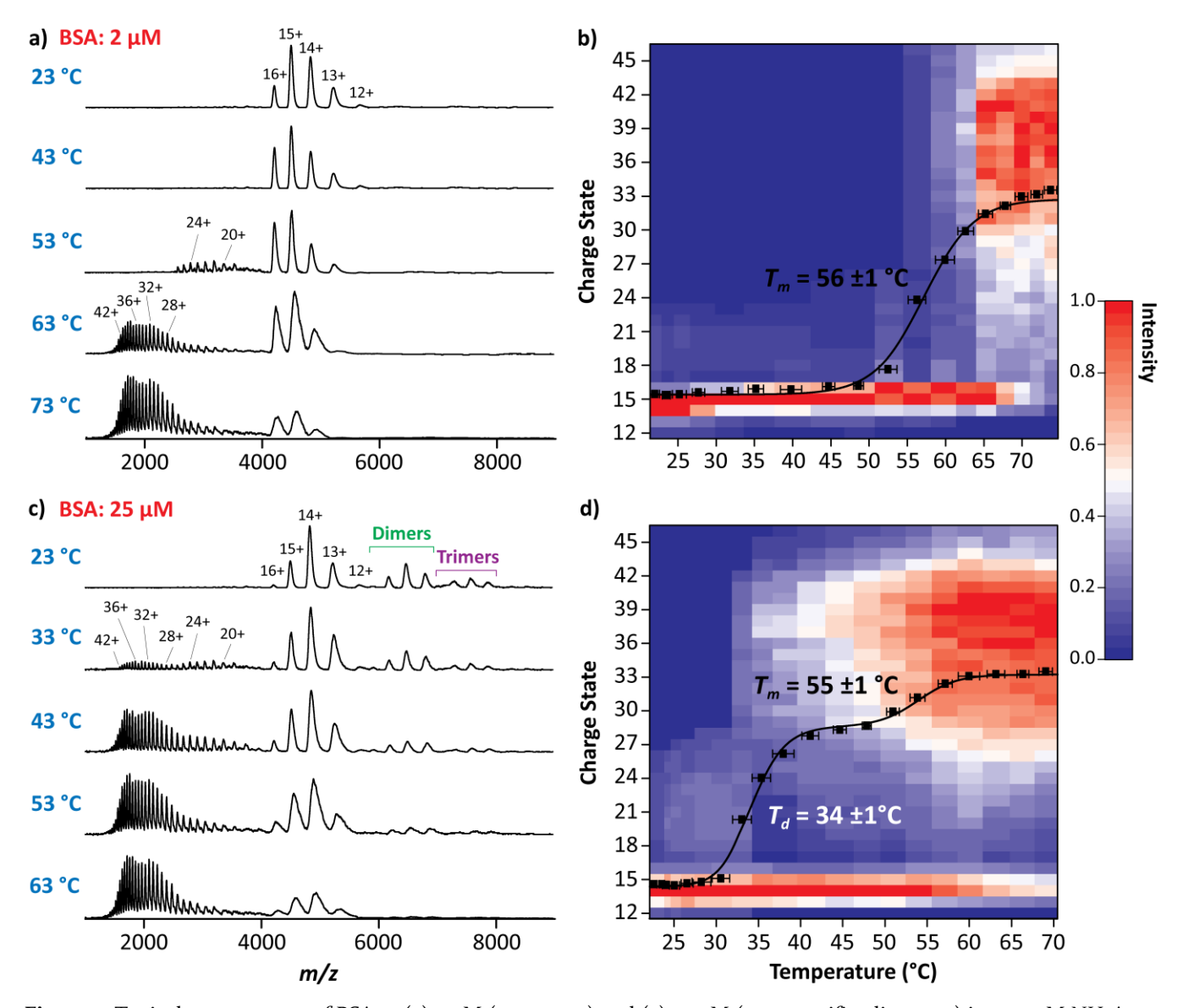


Figure 1. Typical mass spectra of BSA at (a) 2 μ M (monomer) and (c) 25 μ M (non-specific oligomers) in 100 mM NH₄Ac as a function of the starting solution temperature. Heat map of the charge states as a function of the starting solution temperature for BSA at (b) 2 μ M and (d) 25 μ M in 100 mM NH₄Ac. The weighted average charge state (black traces) as a function of the starting solution temperature is shown with a $T_m = 56 \pm 1$ °C for the BSA at 2 μ M (b) and a $T_d = 34 \pm 1$ °C and $T_m = 55 \pm 1$ °C for the BSA at 25 μ M (d).

(Figure 1a). At ~55 °C, a more drastic change in the charge state distribution was obtained reflected by the presence of an additional envelop of charge states centered at 36+ (Figures 1a and 1b). Beyond ~55 °C, a significant increase in the relative abundance of the second envelop of charge states (36+) was observed while the population of the native-like lower charge states diminished (Figures 1a and 1b). Overall, the higher charge states were favored when increasing the starting solution temperatures, for which the $[M+46H]^{46+}$ was the highest observed charge state. A stable nESI signal above ~70 °C was difficult to obtain.

The shift in the charge state distribution can be related to structural changes in the BSA protein structure with the increase in the starting solution temperature leading to denaturing processes where basic sites become accessible for ionization. ^{55, 56} A plot of the weighted average charge state as a function of the starting solution temperature is shown in Figure 1b illustrating the BSA observations at 2 μ M: a single sigmoidal curve (black trace), resembling a typical cooperative two-state unfolding transition ³⁷ with a melting temperature $T_m \sim 56 \pm 1$ °C (Figure 1b). The measured experimental T_m is in good agreement with calorimetry measurements ($T_m = 56$ °C). ⁵⁷ A slight increase in the weighted average charge state was observed near 70 °C; however, instabilities of the nESI

sprayer did not allowed to confirm the second transition reported at T_m = 69 °C.⁵⁷

When the same experiment is performed with BSA at 25 μ M under native starting solution conditions (i.e., 100 mM NH₄Ac), BSA oligomers are observed, an BSA monomer envelope of higher charge states (+36) appears at ~33 °C, and substantially increases in relative intensity with the temperature increase (Figures 1c and 1d). The weighted average charge state plot gave rise to a double sigmoidal curve, with two midpoints representing: i) the BSA oligomer-dissociation temperature $T_d = ~34 \pm 1$ °C corresponding to the dissociation into monomers of higher order BSA oligomers (e.g., dimers and trimers), and ii) the monomeric BSA $T_m = ~55 \pm 1$ °C which highlights the average passage of the native-like states toward the unfolded-like states of BSA (Figure 1d).

CCS distribution dependence with the starting solution temperature. The IMS-MS experiments provide an overview on thermally induced BSA structural changes since only the starting solution temperature was varied. Ions were "softly transferred" into the TIMS analyzer to structural changes via collisions with the bath gas by keeping a low ΔV ($\Delta V = 20$ V) between the deflector (V_{def}) and the funnel entrance (V_{fun}), as well as between the funnel entrance and the TIMS analyzer (V_{ramp}) ; these conditions allow for native-like TIMS measurements. The high trapping efficiency and extended mass range of the second generation TIMS-MS instrument with a convex, quadrupolar electrode geometry,44 enabled the trapping of native-like BSA species at low charge states (+12 to +16). The TIMS profiles of each charge state (+12 to +16) exhibited a single IMS band centered at $\sim 4500 \text{ Å}^2$ (Figure S₃a), indicating that these charge state species correspond to compact structures. In addition, the measured CCS were found consistent with previously reported CCS values using a drift tube IMS.58, 59

Figures 2a-2d display the overall collision cross section (CCS) profiles, which result from the sum of all the observed charge states of BSA. The TIMS profiles of each charge state can be found in Figure S4 for the case of a starting solution temperature at ~63 °C, for which all the charge states are obtained (12+ to 46+). The charge state distribution dependence with the starting solution temperature was accompanied by changes in the TIMS profiles toward higher CCS (Figures 2a-d). In fact, an increase in relative intensity of more unfolded conformations were observed when increasing the starting solution temperature. These IMS profiles confirm that increasing the starting temperature induces changes toward more conformational extended structures while the relative abundance of the native-like conformations was unfavored at high temperature (Figures 2a-d). The weighted average CCS as a function of the starting solution temperature showed a similar profile to that obtained using the charge state distribution, where a T_m ~56 ± 1 °C (Figure 2c) was obtained for the BSA monomer at low concentration (2 μ M), and a T_d ~34 ± 1 °C and T_m = ~55 °C ± 1 °C for the BSA monomer a slightly higher concentration (25 μ M) due to the presence of non-specific oligomers (Figure 2d).

More detailed BSA structural changes can be follow at the charge state and mobility level (Figure S₅). These plots revealed relatively similar trends for the 12+ to 14+, 15+ to 16+, 17+ to 26+ and 27+ to 46+ (Figure S₅) states. Figures 2e and 2f display the sum profiles in relative abundance of the 12+ to 14+ (black squares), 15+ to 16+ (magenta diamonds), 17+ to 26+ (red circles) and 27+ to 46+ (blue triangles) charge states at 2 μ M and 25 μ M BSA, respectively.

For the 2 µM BSA solution, the relative abundance of the native-like states (12+ to 14+) started to decrease around ~28 °C, while the populations of the 15+ and 16+ increased (Figure 2e). The same trend but less pronounced was observed until ~51 °C, where both 12+ to 14+ and 15+ to 16+ decreased while the populations of more extended states (17+ to 26+) increased (Figure 2e). At ~57 °C, a substantial increase of more extended conformations (27+ to 46+) was observed (blue trace in Figure 2e). These plots led to the observation of several structural transitions: (1) at ~27 °C which highlights the passage from the native-like states (12+ to 14+) to a first native intermediate (15+ to 16+) with similar CCS that become more favored; (2) at ~37 °C, a second native intermediate is observed which still displays similar CCS but with a slight broadening in the IMS profiles; (3) at ~51 °C, which highlights the passage from the native intermediates to more extended structures (17+ to 26+); (4) at ~57 °C, which highlights the passage from the extended conformations to the unfolded states (27+ to 46+) with higher CCS; Finally, two new transitions at (5) ~62 °C and (6) ~66 °C were observed corresponding to the most thermally stable structures of the unfolded states.

For the 25 μ M BSA solution, similar trends in relative abundance with respect to the 2 μ M BSA were observed for the 12+ to 14+ and 15+ to 16+ (Figure 2f). However, an increase of the 17+ to 26+ and 27+ to 46+ was obtained at ~27 °C and near T_d , respectively (Figure 2f). These plots suggest that the presence of oligomers may have an impact on the determination of melting temperatures as well as on the assignment of unfolding transitions as the dissociation of oligomers may produce monomers with more extended structures than those expected at that solution temperature.

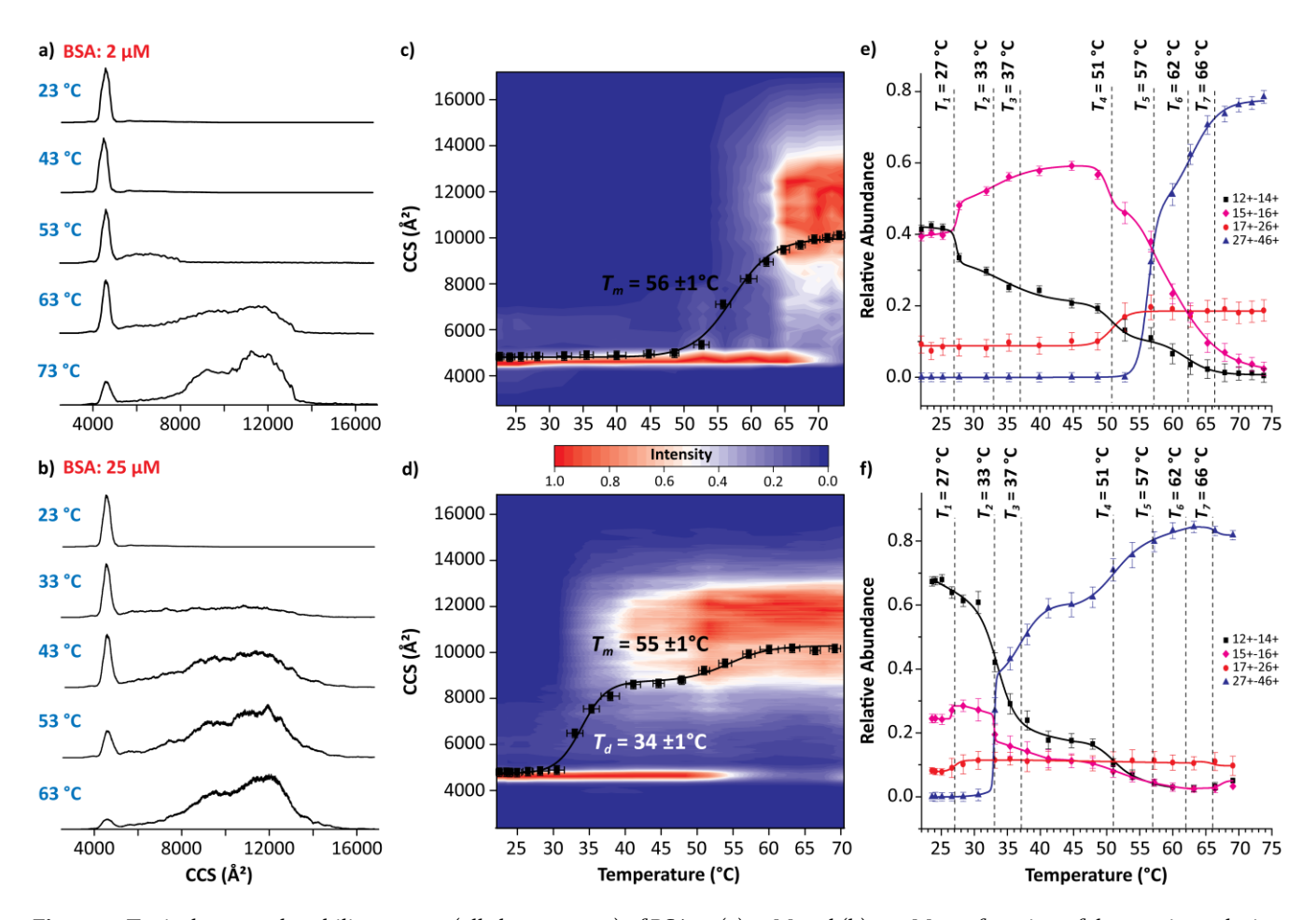


Figure 2. Typical summed mobility spectra (all charge states) of BSA at (a) 2μM and (b) 25 μM as a function of the starting solution temperature. Heat map of the CCS as a function of the starting solution temperature for BSA at (c) 2 μM and (d) 25 μM. The weighted average CCS (black traces) as a function of the starting solution temperature showing a $T_m = 56 \pm 1$ °C for the BSA monomer (c) and a $T_d = 34 \pm 1$ °C and $T_m = 55 \pm 1$ °C in the presence of BSA non-specific oligomers (d), respectively. Plot representing the relative abundances of the 12+ to 14+ (black squares), 15+ to 16+ (magenta diamonds), 17+ to 26+ (red circles) and 27+ to 46+ (blue triangles) charge states of BSA at (e) 2 μM and (f) 25 μM as a function of the starting solution temperatures.

The IMS profiles generated from the 2 µM BSA solution during native solvent conditions did not showed additional features with the increase of the starting solution temperature. For example, the TIMS profiles of the native-like ions (e.g., $[M + 14H]^{14+}$ ions) consisted of a single, narrow IMS band at ~ 4500 Å² and only exhibited a decrease in relative abundance with the temperature increase (Figure 3a). However, most of the TIMS profiles of higher charge states showed more broad and heterogeneous mobility profiles accompanied by changes in their relative abundances with the starting solution temperature increase. For example, the CCS distribution of the $[M + 25H]^{25+}$ ions at 23 °C presented a broad IMS distribution with at least three distinct features (IMS bands 1-3, Figure 3b). The total abundance of the [M + 25H]²⁵⁺ ions remained relatively unchanged from 33 to 70

°C, while the IMS profile exhibited a conformational shift toward higher CCS values. As the temperature increased close to T_d (~ 33 °C), a change in the relative intensity was observed between IMS bands 2 and 3, for which the IMS band 3 (higher CCS) become more abundant than the IMS band 2 (Figure 3b). In addition, the IMS band 3 remained predominant until approaching T_m (~ 53 °C), where the IMS band 4 was more favored. The changes close to T_d (~ 33 °C) include the contribution of the thermally dissociated dimer and trimer into monomer species. Inspection of the IMS profiles shows that rather than dissociating into a native like structure, the oligomers dissociate to a more extended structure (e.g., IMS band 4); these is in good agreement with the shift toward higher charge states observed at T_d . The IMS band 4 was the most abundant conformation from T_m to 70 °C. Note that two additional features at higher CCS (IMS bands 5 and 6) were also observed with the solution temperature increase (Figure 3b). These observations describe the minimum number of structural intermediates involved in the transition from native to unfolded states of BSA.

The IMS profiles of the $[M + 38H]^{38+}$ ions, which are part of the unfolded states of BSA and only obtained near T_d , did not exhibit additional features when increasing the starting solution temperature (Figure 3c). However, the CCS distributions, for which a broad IMS distribution including at least six distinct conformations (IMS bands A-F), also showed changes in the relative abundance

favoring higher CCS with the starting solution temperature increase (Figure 3c). The IMS band C was predominant around T_d , while the IMS band D with higher CCS was favored above T_d at 43 °C (Figure 3c). The IMS band D remained predominant until reaching T_m (\sim 53 °C), where the IMS band E was more favored. The IMS band E was found the most abundant conformation as the temperature increased above T_m (Figure 3c). These observations also support the hypothesis that multiple structural intermediates are present and provides a minimum number of transitions. The reproducibility of these structural transitions was confirmed during replicate experiments (Figure S6).

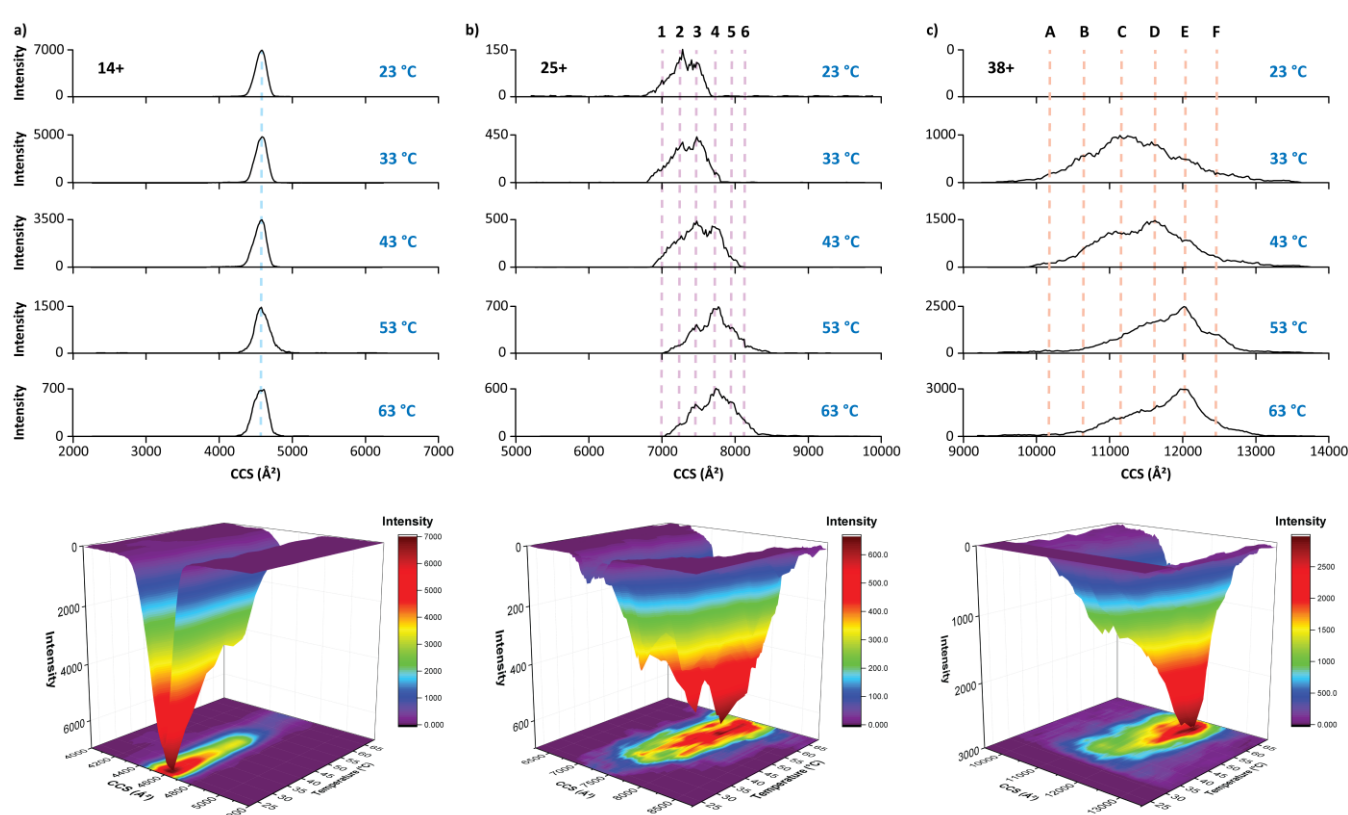


Figure 3. TIMS-MS analysis showing the CCS profiles at selected starting solution temperature and 3D free energy protein landscape (mobility vs solution temperature vs relative intensity) as a function of the protein charge state for the (a) $[M + 14H]^{14+}$, (b) $[M + 25H]^{25+}$ and (c) $[M + 38H]^{38+}$ ions. The colored dashed line illustrated the position of the identified IMS bands.

Non-specific BSA oligomer dependence with the starting solution temperature. The BSA 25 μ M concentration solution condition also resulted in the presence of non-specific dimeric and trimeric species of BSA in native starting solution conditions (i.e., 100 mM NH₄Ac at 23 °C, Figure S₃a). In fact, TIMS-MS analysis for BSA oligomers exhibited a narrow charge state distribution, ranging from $[2M + 20H]^{20+}$ to $[2M + 23H]^{23+}$ and $[3M + 26H]^{26+}$ to $[3M + 29H]^{29+}$, for BSA dimers and trimers, respectively. The TIMS-MS experiments of BSA

dimers and trimers displayed a charge state distribution dependence with increasing the starting solution temperatures that was different from the one observed for the monomeric species. While the same charge state distribution was observed when increasing the starting solution temperature, only a sharp decrease in the relative abundance was obtained for BSA dimers (Figure 4a) and trimers (Figure 4b) relative to their dissociation into monomeric species at T_d . The signal of BSA dimers and trimers completely disappeared as the starting

solution temperature was raised near the BSA monomeric T_m . These curves typically resembled to a cooperative two-state melting transition,^{37, 60} yielding a T_m at ~ 33 °C (± 1 °C) and ~ 35 °C (± 1 °C) for both BSA dimers and trimers, respectively (Figure 4) These two melting points are within the error of the oligomer-dissociation temperature T_d observed in the BSA monomeric distribution.

The IMS profiles of the BSA dimers (Figure S₃b) and trimers (Figure S₃c) presented a single IMS band for all the charge state observed. In the solution temperature range studied, no changes in the CCS distribution were observed. This result suggests that rather than inducing a non-asymmetric conformational change at the constituent level in the oligomer, the system is thermalized leading to the rupture of the intermolecular interactions that stabilize the oligomers. Inspection of the 3D free energy protein landscape (mobility vs solution temperature vs relative intensity) as a function of the charge state (Figure 4) showed a very narrow landscape profile fort the case of dimer and trimer as expected. In the case of the presence of oligomers, one of the main conclusions is that weak oligomer interaction can affect the monitoring of the monomer BSA melting experiment by introducing an early inflection point, not relative to the monomer but to the dissociation of the oligomers (as shown in Figures 1d, 2d and 2f). This observation is common to any IMS-MS instrumentation that does not have pre-selection prior to the mobility analyzer. It is known that weakly bound oligomers can easily dissociate into monomers in the IMS-MS interface and they will be observed as monomers in the MS, but they will be recorded in the IMS profiles as oligomers, potentially introducing artifacts in the analysis. The present example shows that proper tuning of the TIMS-MS allows to differentiate the two cases. While it was illustrated for the case of a homo- dimer and trimer, future work will be applied to the screening of weakly bound protein-ligand and protein-protein complexes.

CONCLUSION

A variable temperature nESI source was coupled for the first time to a trapped ion mobility spectrometry - mass spectrometry for the study of solution based thermally induced transitions. The high speed of the IMS-MS acquisition (e.g., ~100-200 ms per analysis) allows to efficiently sample a solution temperature gradient (~23-70 °C in few of minutes). A good correspondence was observed between the trends observed in the IMS and MS domain; i.e., the T_m measure from the average charge and CCS distributions suggested a two-state unfolding transition with a melting temperature $Tm \sim 56 \pm 1$ °C; however, the inspection of the CCS profiles at the charge

state level as a function of the solution temperature showcase at least six structural transitions (T1-T7).

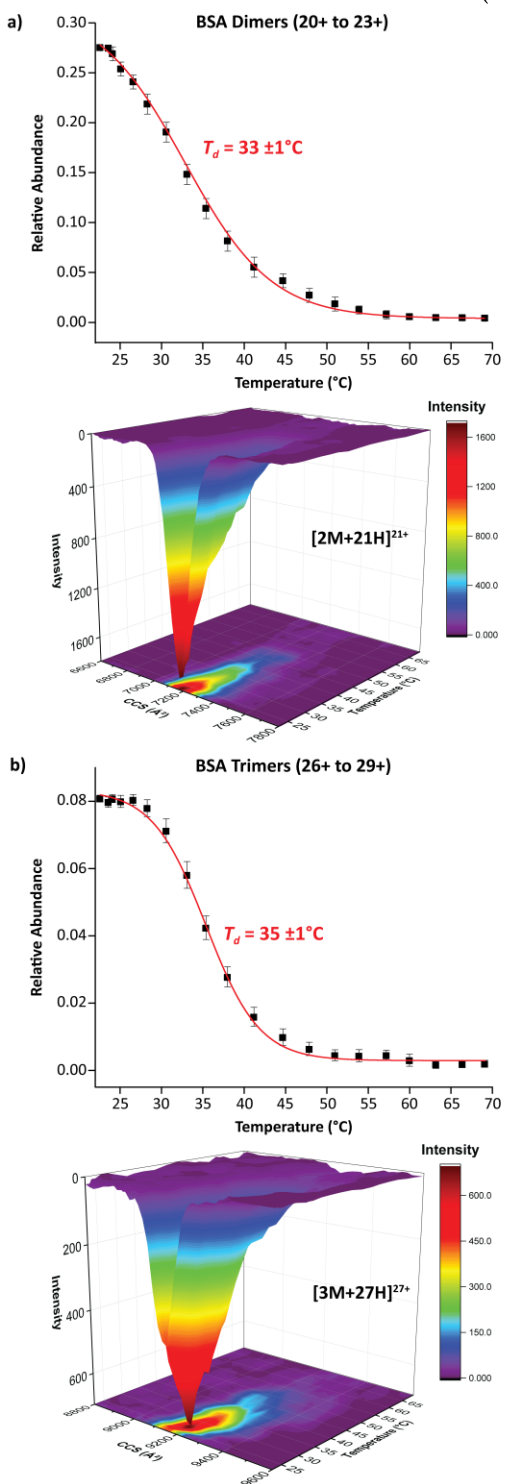


Figure 4. TIMS-MS analysis showing a plot of the relative abundances of the sum of all charge states and CCS profiles at a specific charge state as a function of the temperature for the (a) dimeric and (b) trimeric species of BSA.

If the starting solution concentration is slightly increased (from 2 to 25 μ M), this method can detect non-specific BSA dimers and trimers who dissociate early ($T_d \sim 34 \pm 1$ °C) and may disturb the melting curve of the BSA monomer.

The TIMS-MS experiments provide additional information about the complexity associated with a thermally induced transition involving many states, which can be dissected at the level of charge state and IMS band. These experiments enabled us to outline a more detailed description of the structural landscape associated with a protein denaturing process in solution. While this work focuses on the case of a single protein, this technology could be easily translated to the study of protein-ligand and protein-protein complexes in solution.

ASSOCIATED CONTENT

Supporting Information

TIMS-MS instrument showing the schematic of the temperature-controlled nESI ionization source with the TIMS cell and TIMS operation. Plot representing the evolution of temperature as a function of time for BSA at 2 μ M and 25 μ M. Native TIMS spectra of the multiply protonated species of BSA monomers, BSA dimers and BSA trimers in native starting solution conditions. Typical TIMS profiles for the multiply protonated species of BSA obtained at 63 °C. Plots representing the relative abundances for each charge state of BSA as a function of the starting solution temperatures. Replicates of the TIMS profiles as a function of the starting solution temperature for the [M + 25H]²⁵⁺ and [M + 38H]³⁸⁺ ions. This material is available free of charge via the Internet at http://pubs.acs.org.

AUTHOR INFORMATION

Corresponding Author

fernandf@fiu.edu

Notes

The authors declare no competing financial interest.

ACKNOWLEDGEMENTS

The authors acknowledge the financial support from the National Science Foundation Division of Chemistry, under CAREER award CHE-1654274, with co-funding from the Division of Molecular and Cellular Biosciences to FFL and funding from National Institutes of General Medicine (Ro1GM134247).

REFERENCES

1. Dill, K. A.; Shortle, D., Denatured states of proteins. *Annu. Rev. Biochem.* **1991**, *60*, 795-825.

- 2. Myers, J. K.; Pace, C. N.; Scholtz, J. M., Denaturant m values and heat capacity changes: relation to changes in accessible surface areas of protein unfolding. *Protein Sci.* **1995**, *4* (10), 2138-2148.
- 3. Bennion, B. J.; Daggett, V., The molecular basis for the chemical denaturation of proteins by urea. *Proc. Natl. Acad. Sci. USA.* **2003**, 100 (9), 5142-5147.
- 4. Anderson, D. E.; Becktel, W. J.; Dahlquist, F. W., pH-induced denaturation of proteins: a single salt bridge contributes 3-5 kcal/mol to the free energy of folding of T4 lysozyme. *Biochemistry* **1990**, 29 (9), 2403-2408.
- 5. Kishore, D.; Kundu, S.; Kayastha, A. M., Thermal, chemical and pH induced denaturation of a multimeric betagalactosidase reveals multiple unfolding pathways. *PloS One* **2012**, *7* (11), e50380.
- 6. Mitaku, S.; Ikuta, K.; Itoh, H.; Kataoka, R.; Naka, M.; Yamada, M.; Suwa, M., Denaturation of bacteriorhodopsin by organic solvents. *Biophys. Chem.* **1988**, 30 (1), 69-79.
- 7. Jackson, S. E.; Fersht, A. R., Folding of chymotrypsin inhibitor 2. 1. Evidence for a two-state transition. *Biochemistry* **1991**, 30 (43), 10428-10435.
- 8. Weijers, M.; Barneveld, P. A.; Cohen Stuart, M. A.; Visschers, R. W., Heat-induced denaturation and aggregation of ovalbumin at neutral pH described by irreversible first-order kinetics. *Protein Sci.* **2003**, *12* (12), 2693-2703.
- 9. Lepock, J. R., Measurement of protein stability and protein denaturation in cells using differential scanning calorimetry. *Methods* **2005**, 35 (2), 117-125.
- 10. Schon, A.; Clarkson, B. R.; Jaime, M.; Freire, E., Temperature stability of proteins: Analysis of irreversible denaturation using isothermal calorimetry. *Proteins* **2017**, *85* (11), 2009-2016.
- 11. Chen, H.; Rhoades, E., Fluorescence characterization of denatured proteins. *Curr. Opin. Struct. Biol.* **2008**, *18* (4), 516-524.
- 12. Sherman, E.; Itkin, A.; Kuttner, Y. Y.; Rhoades, E.; Amir, D.; Haas, E.; Haran, G., Using fluorescence correlation spectroscopy to study conformational changes in denatured proteins. *Biophys. J.* **2008**, *94* (12), 4819-4827.
- 13. Greenfield, N. J., Using circular dichroism collected as a function of temperature to determine the thermodynamics of protein unfolding and binding interactions. *Nat. Protoc.* **2006**, *1* (6), 2527-2535.
- 14. Lamba, J.; Paul, S.; Hasija, V.; Aggarwal, R.; Chaudhuri, T. K., Monitoring protein folding and unfolding pathways through surface hydrophobicity changes using fluorescence and circular dichroism spectroscopy. *Biochemistry* **2009**, *74* (4), 393-398.
- 15. Dyson, H. J.; Wright, P. E., Unfolded proteins and protein folding studied by NMR. *Chem. Rev.* **2004**, *104* (8), 3607-3622.
- 16. Gupta, S.; Bhattacharjya, S., NMR characterization of the near native and unfolded states of the PTB domain of Dok: alternate conformations and residual clusters. *PloS One* **2014**, *9* (2), e90557.
- 17. Chowdhury, S. K.; Katta, V.; Chait, B. T., Probing conformational changes in proteins by mass spectrometry. *J. Am. Chem. Soc.* **1990**, *112* (24), 9012-9013.
- 18. Loo, J. A.; Loo, R. R.; Udseth, H. R.; Edmonds, C. G.; Smith, R. D., Solvent-induced conformational changes of polypeptides probed by electrospray-ionization mass

- spectrometry. Rapid Commun. Mass Spectrom. 1991, 5 (3), 101-105.
- 19. Konermann, L.; Douglas, D. J., Unfolding of proteins monitored by electrospray ionization mass spectrometry: a comparison of positive and negative ion modes. *J. Am. Soc. Mass Spectrom.* **1998**, *9* (12), 1248-1254.
- 20. Blanc, J. C. Y. L.; Beuchemin, D.; Siu, K. W. M.; Guevremont, R.; Berman, S. S., Thermal denaturation of some proteins and its effect on their electrospray mass spectrat. *Organic Mass Spectrom.* **1991**, *26* (10), 831-839.
- 21. Mirza, U. A.; Cohen, S. L.; Chait, B. T., Heat-induced conformational changes in proteins studied by electrospray ionization mass spectrometry. *Anal. Chem.* **1993**, *65* (1), 1-6.
- 22. Daneshfar, R.; Kitova, E. N.; Klassen, J. S., Determination of Protein-Ligand Association Thermochemistry Using Variable-Temperature Nanoelectrospray Mass Spectrometry. *J. Am. Chem. Soc.* 2004, 126 (15), 4786-4787.
- 23. Benesch, J. L.; Sobott, F.; Robinson, C. V., Thermal dissociation of multimeric protein complexes by using nanoelectrospray mass spectrometry. *Anal. Chem.* 2003, 75 (10), 2208-2214.
- 24. Wang, G.; Abzalimov, R. R.; Kaltashov, I. A., Direct monitoring of heat-stressed biopolymers with temperature-controlled electrospray ionization mass spectrometry. *Anal. Chem.* **2011**, *8*3 (8), 2870-2876.
- 25. Cong, X.; Liu, Y.; Liu, W.; Liang, X.; Russell, D. H.; Laganowsky, A., Determining Membrane Protein-Lipid Binding Thermodynamics Using Native Mass Spectrometry. *J. Am. Chem. Soc.* **2016**, *1*38 (13), 4346-4349.
- 26. Vahidi, S.; Stocks, B. B.; Konermann, L., Partially disordered proteins studied by ion mobility-mass spectrometry: implications for the preservation of solution phase structure in the gas phase. *Anal. Chem.* 2013, 85 (21), 10471-10478.
- 27. Butcher, D.; Bernad, S.; Derrien, V.; Sebban, P.; Miksovska, J.; Fernandez-Lima, F., Non-symbiotic hemoglobin conformational space dependence on the heme coordination using nESI-TIMS-TOF MS. *Int. J. Mass Spectrom.* **2018**, *43*0, 37-43.
- 28. Smith, D. P.; Giles, K.; Bateman, R. H.; Radford, S. E.; Ashcroft, A. E., Monitoring copopulated conformational states during protein folding events using electrospray ionization-ion mobility spectrometry-mass spectrometry. *J. Am. Soc. Mass Spectrom.* 2007, *18* (12), 2180-2190.
- 29. Litwinczuk, A.; Ryu, S. R.; Nafie, L. A.; Lee, J. W.; Kim, H. I.; Jung, Y. M.; Czarnik-Matusewicz, B., The transition from the native to the acid-state characterized by multi-spectroscopy approach: study for the holo-form of bovine alpha-lactalbumin. *Biochim. Biophys. Acta* **2014**, *1844* (3), 593-606.
- 30. Pierson, N. A.; Chen, L.; Valentine, S. J.; Russell, D. H.; Clemmer, D. E., Number of solution states of bradykinin from ion mobility and mass spectrometry measurements. *J. Am. Chem. Soc.* **2011**, *1*33 (35), 13810-13813.
- 31. El-Baba, T. J.; Fuller, D. R.; Hales, D. A.; Russell, D. H.; Clemmer, D. E., Solvent Mediation of Peptide Conformations: Polyproline Structures in Water, Methanol, Ethanol, and 1-Propanol as Determined by Ion Mobility Spectrometry-Mass Spectrometry. *J. Am. Soc. Mass Spectrom.* 2019, 30 (1), 77-84.
- 32. Shi, H.; Clemmer, D. E., Evidence for two new solution states of ubiquitin by IMS-MS analysis. *J. Phys. Chem. B* **2014**, *118* (13), 3498-3506.

- 33. Butcher, D.; Miksovska, J.; Ridgeway, M. E.; Park, M. A.; Fernandez-Lima, F., The effects of solution additives and gas-phase modifiers on the molecular environment and conformational space of common heme proteins. *Rapid Commun. Mass Spectrom.* **2019**, 33 (5), 399-404.
- 34. Jeanne Dit Fouque, K.; Moreno, J.; Fernandez-Lima, F., Exploring the Conformational Space of Growth-Hormone-Releasing Hormone Analogues Using Dopant Assisted Trapped Ion Mobility Spectrometry-Mass Spectrometry. *J. Phys. Chem. B* **2019**, *12*3 (29), 6169-6177.
- 35. Meyer, N. A.; Root, K.; Zenobi, R.; Vidal-de-Miguel, G., Gas-Phase Dopant-Induced Conformational Changes Monitored with Transversal Modulation Ion Mobility Spectrometry. *Anal. Chem.* 2016, 88 (4), 2033-2040.
- 36. Hommersom, B.; Porta, T.; Heeren, R. M. A., Ion mobility spectrometry reveals intermediate states in temperature-resolved DNA unfolding. *Int. J. Mass Spectrom.* **2017**, *419*, 52-55.
- 37. El-Baba, T. J.; Woodall, D. W.; Raab, S. A.; Fuller, D. R.; Laganowsky, A.; Russell, D. H.; Clemmer, D. E., Melting Proteins: Evidence for Multiple Stable Structures upon Thermal Denaturation of Native Ubiquitin from Ion Mobility Spectrometry-Mass Spectrometry Measurements. *J. Am. Chem. Soc.* 2017, 139 (18), 6306-6309.
- 38. Brown, C. J.; Woodall, D. W.; El-Baba, T. J.; Clemmer, D. E., Characterizing Thermal Transitions of IgG with Mass Spectrometry. *J. Am. Soc. Mass Spectrom.* 2019.
- 39. Jeanne Dit Fouque, K.; Bisram, V.; Hegemann, J. D.; Zirah, S.; Rebuffat, S.; Fernandez-Lima, F., Structural signatures of the class III lasso peptide BI-32169 and the branched-cyclic topoisomers using trapped ion mobility spectrometry-mass spectrometry and tandem mass spectrometry. *Anal. Bioanal. Chem.* 2019, 411 (24), 6287-6296.
- 40. Woodall, D. W.; El-Baba, T. J.; Fuller, D. R.; Liu, W.; Brown, C. J.; Laganowsky, A.; Russell, D. H.; Clemmer, D. E., Variable-Temperature ESI-IMS-MS Analysis of Myohemerythrin Reveals Ligand Losses, Unfolding, and a Non-Native Disulfide Bond. *Anal. Chem.* 2019, 91 (10), 6808-6814.
- 41. El-Baba, T. J.; Clemmer, D. E., Solution thermochemistry of concanavalin A tetramer conformers measured by variable-temperature ESI-IMS-MS. *Int. J. Mass Spectrom.* **2019**, 443, 93-100.
- 42. Pacholarz, K. J.; Barran, P. E., Distinguishing Loss of Structure from Subunit Dissociation for Protein Complexes with Variable Temperature Ion Mobility Mass Spectrometry. *Anal. Chem.* **2015**, *87* (12), 6271-6279.
- 43. Ujma, J.; Giles, K.; Morris, M.; Barran, P. E., New High Resolution Ion Mobility Mass Spectrometer Capable of Measurements of Collision Cross Sections from 150 to 520 K. *Anal. Chem.* **2016**, 88 (19), 9469-9478.
- 44. Jeanne Dit Fouque, K.; Fernandez-Lima, F., Recent advances in biological separations using trapped ion mobility spectrometry mass spectrometry. *Trends Anal. Chem.* **2019**, *116*, 308-315.
- 45. Jeanne Dit Fouque, K.; Garabedian, A.; Leng, F.; Tse-Dinh, Y. C.; Fernandez-Lima, F., Microheterogeneity of Topoisomerase IA/IB and Their DNA-Bound States. *ACS Omega* **2019**, *4* (2), 3619-3626.
- 46. Koleva, B. N.; Gokcan, H.; Rizzo, A. A.; Lim, S.; Jeanne Dit Fouque, K.; Choy, A.; Liriano, M. L.; Fernandez-Lima, F.; Korzhnev, D. M.; Cisneros, G. A.; Beuning, P. J., Dynamics of the

- E. coli beta-Clamp Dimer Interface and Its Influence on DNA Loading. *Biophys. J.* **2019**, *117* (3), 587-601.
- 47. Fernandez-Lima, F. A.; Kaplan, D. A.; Park, M. A., Note: Integration of trapped ion mobility spectrometry with mass spectrometry. *Rev. Sci. Instrum.* **2011**, 82 (12), 126106.
- 48. Fernandez-Lima, F. A.; Kaplan, D. A.; Suetering, J.; Park, M. A., Gas-phase separation using a Trapped Ion Mobility Spectrometer. *Int. J. Ion Mobil. Spectrom.* **2011**, *14* (2-3), 93-98.
- 49. Liu, F. C.; Kirk, S. R.; Bleiholder, C., On the structural denaturation of biological analytes in trapped ion mobility spectrometry mass spectrometry. *Analyst* **2016**, *141* (12), 3722-3730.
- 50. Hernandez, D. R.; Debord, J. D.; Ridgeway, M. E.; Kaplan, D. A.; Park, M. A.; Fernandez-Lima, F., Ion dynamics in a trapped ion mobility spectrometer. *Analyst* **2014**, *139* (8), 1913-1921.
- 51. Ridgeway, M. E.; Lubeck, M.; Jordens, J.; Mann, M.; Park, M. A., Trapped ion mobility spectrometry: A short review. *Int. J. Mass Spectrom.* **2018**, 425, 22-35.
- 52. Michelmann, K.; Silveira, J. A.; Ridgeway, M. E.; Park, M. A., Fundamentals of trapped ion mobility spectrometry. *J. Am. Soc. Mass Spectrom.* **2015**, 26 (1), 14-24.
- 53. Silveira, J. A.; Michelmann, K.; Ridgeway, M. E.; Park, M. A., Fundamentals of Trapped Ion Mobility Spectrometry Part II: Fluid Dynamics. *J. Am. Soc. Mass Spectrom.* **2016**, *27* (4), 585-595.
- 54. Revercomb, H. E.; Mason, E. A., Theory of plasma chromatography/gaseous electrophoresis. Review. *Anal. Chem.* **1975**, 47 (7), 970-983.
- 55. Borzova, V. A.; Markossian, K. A.; Chebotareva, N. A.; Kleymenov, S. Y.; Poliansky, N. B.; Muranov, K. O.; Stein-Margolina, V. A.; Shubin, V. V.; Markov, D. I.; Kurganov, B. I., Kinetics of Thermal Denaturation and Aggregation of Bovine Serum Albumin. *PloS One* **2016**, *11* (4), e0153495.
- 56. Molodenskiy, D.; Shirshin, E.; Tikhonova, T.; Gruzinov, A.; Peters, G.; Spinozzi, F., Thermally induced conformational changes and protein-protein interactions of bovine serum albumin in aqueous solution under different pH and ionic strengths as revealed by SAXS measurements. *Phys. Chem. Chem. Phys.* **2017**, *19* (26), 17143-17155.
- 57. Michnik, A., *J. Therm. Anal. Calorim.* **2003**, *71* (2), 509-519.
- 58. Bush, M. F.; Hall, Z.; Giles, K.; Hoyes, J.; Robinson, C. V.; Ruotolo, B. T., Collision cross sections of proteins and their complexes: a calibration framework and database for gas-phase structural biology. *Anal. Chem.* **2010**, *82* (22), 9557-9565.
- 59. Harrison, J. A.; Kelso, C.; Pukala, T. L.; Beck, J. L., Conditions for Analysis of Native Protein Structures Using Uniform Field Drift Tube Ion Mobility Mass Spectrometry and Characterization of Stable Calibrants for TWIM-MS. *J. Am. Soc. Mass Spectrom.* 2019, 30 (2), 256-267.
- 6o. Prabhu, N. V.; Sharp, K. A., Heat capacity in proteins. *Annu. Rev. Phys. Chem.* **2005**, *56*, 521-548.

For Table of Contents Only

